online data

Role of the cysteine residues in *Arabidopsis thaliana* cyclophilin CYP20-3 in peptidyl-prolyl *cis–trans* isomerase and redox-related functions

Miriam LAXA*, Janine KÖNIG*†, Karl-Josef DIETZ*[1] and Andrea KANDLBINDER*

*Biochemistry and Physiology of Plants, Faculty of Biology, W5, Bielefeld University, 33501 Bielefeld, Germany, and †Division of Biological Chemistry and Molecular Microbiology, The Wellcome Trust Biocentre, University of Dundee, Dundee DD1 5EH, U.K.

Cyps (cyclophilins) are ubiquitous proteins of the immunophilin superfamily with proposed functions in protein folding, protein degradation, stress response and signal transduction. Conserved cysteine residues further suggest a role in redox regulation. In order to get insight into the conformational change mechanism and functional properties of the chloroplast-located CYP20-3, site-directed mutagenized cysteine → serine variants were generated and analysed for enzymatic and conformational properties under reducing and oxidizing conditions. Compared with the wild-type form, elimination of three out of the four cysteine residues decreased the catalytic efficiency of PPI (peptidyl-prolyl *cis–trans* isomerase) activity of the reduced CYP20-3, indicating a regulatory role of dithiol–disulfide transitions in protein function. Oxidation was accompanied by conformational changes with a predominant role in the structural rearrangement of the disulfide bridge formed between Cys^{54} and Cys^{171}. The rather negative E_m (midpoint redox potential) of −319 mV places CYP20-3 into the redox hierarchy of the chloroplast, suggesting the activation of CYP20-3 in the light under conditions of limited acceptor availability for photosynthesis as realized under environmental stress. Chloroplast Prx (peroxiredoxins) were identified as interacting partners of CYP20-3 in a DNA-protection assay. A catalytic role in the reduction of 2-Cys PrxA and 2-Cys PrxB was assigned to Cys^{129} and Cys^{171}. In addition, it was shown that the isomerization and disulfide-reduction activities are two independent functions of CYP20-3 that both are regulated by the redox state of its active centre.

Key words: *Arabidopsis thaliana*, chloroplast, cyclophilin, immunophilin, peptidyl-prolyl *cis–trans* isomerase (PPI), peroxiredoxin.

INTRODUCTION

Cyps (cyclophilins) are members of the immunophilin protein superfamily. The *Arabidopsis* genome encodes at least 52 genes for immunophilins, immunophilin-like proteins and multidomain proteins with immunophilin domains [1]. Thus plants possess the largest number of immunophilin family members as compared with other organisms with sequenced genomes at present [2]. Among these, 29 gene products belong to the Cyp subfamily [3]. The functions of the plant Cyps mostly are unknown and unexplored. In mammals, they were first identified as targets of the immunosuppressive drug CsA (cyclosporin A) [4]. They constitute a family of phylogenetically old proteins occurring ubiquitously in bacteria, animals and plants [1,3,5] where they are known for their function in the isomerization of Xaa–Pro peptide bonds during the folding and assembly of proteins. Furthermore, they act as chaperones [6–11] and are involved in regulatory signal transduction pathways [2,12,13] during stress responses [14–16], plant development [17] and affect RNA splicing reactions [5,18,19]. Lee et al. [20] observed the binding of human CypA to human peroxiredoxins Prx I–VI by MALDI–TOF (matrix-assisted laser-desorption ionization–time-of-flight) analysis and confirmed it via protein overlay assays and subsequent Western immunoblot analysis. Recently, it was shown in a DNA-protection assay that a Cyp from *Pisum sativum* is able to reduce oxidized 2-Cys Prx and regenerates the peroxide-detoxifying activity [21]. The reaction mechanism is still unclear.

Plant peroxiredoxins are non-haem-containing peroxidases [22,23]. They detoxify H_2O_2 (hydrogen peroxide), alkyl hydroperoxides and peroxynitrite [24–26]. The active centre contains a conserved cysteine residue, which reduces different peroxides. Its regeneration is coupled with electron donors such as thioredoxins, glutaredoxins and Cyps [21,26]. Prxs are grouped into four clans, namely 1-Cys Prx, 2-Cys Prx, type-II Prx and PrxQ, according to sequence similarities, presence of an additional resolving cysteinyl group at variable positions, as well as the mechanisms of catalysis and regeneration [23,25]. The *Arabidopsis thaliana* genome encodes ten different Prxs with distinct subcellular localization, tissue distribution, transcriptional regulation and biochemical properties [22,27]. Prxs play a role in the antioxidative protection system of photosynthesis, respiration and stress response. Additional functions are proposed in signal transduction during plant development and adaptation [24,25,27].

The 28.2 kDa Cyp CYP20-3 [TAIR (The *Arabidopsis* Information Resource) accession number at3g62030; also termed Roc4] has been characterized previously. It is located in the stroma of chloroplasts [3,28,29] and the four conserved amino acids Arg^{69}, Phe^{74}, Trp^{135} and His^{140} (RFWH motif) are involved in PPI (peptidyl-prolyl *cis–trans* isomerase) activity and CsA binding (tryptophan), implying a function in protein folding. From transcript analyses, a role in protein unfolding and degradation has been proposed under stress conditions such as heat shock [3]. Additionally, it was identified as a target protein for chloroplast Trx-m (thioredoxin m-type) [30,31]. CYP20-3 contains four cysteine residues, which form two disulfide bonds under oxidizing

Abbreviations used: CsA, cyclosporin A; Cyp, cyclophilin; DTNB, 5,5′-dithiobis-(2-nitrobenzoic acid); DTT, dithiothreitol; E_m, midpoint redox potential; MALDI–TOF, matrix-assisted laser-desorption ionization–time-of-flight; PPI, peptidyl-prolyl *cis–trans* isomerase; Prx, peroxiredoxin; ROS, reactive oxygen species; Trx-m, thioredoxin m-type; WT, wild-type.

[1] To whom correspondence should be addressed (email karl-josef.dietz@uni-bielefeld.de).

conditions, namely Cys^{54}–Cys^{171} and Cys^{129}–Cys^{176}, indicating redox-dependent conformational changes shown by DTNB [5,5′-dithiobis-(2-nitrobenzoic acid)] binding and MALDI–TOF MS [31].

The present study aims at improving our understanding of the recently found redox properties of CYP20-3 and its interaction with the different chloroplast-located peroxiredoxins. To this end, each cysteine residue of CYP20-3 was mutagenized and the variants were heterologously expressed in *Escherichia coli*. His-tagged variants as well as the wild-type protein were analysed for PPI activity, redox-dependent electrophoretic mobility using band-shift experiments as well as for their redox-dependent conformational changes by intrinsic tryptophan fluorescence analysis. The E_m (midpoint redox potential) of wild-type and variant proteins was determined to place CYP20-3 into the redox system of the plastids. Furthermore, the disulfide-reducing property of CYP20-3 was analysed in DNA-protection assays with all four chloroplast-located peroxiredoxins.

MATERIALS AND METHODS

RNA isolation and cDNA synthesis

Total RNA was isolated from rosette leaves of *A. thaliana* (ecotype Col-0) plants grown in soil culture (1:1:1 mixture of Frühsdorfer Erde Klocke P, perlite and vermiculite) in a controlled environment (10 h of light, 100 μmol of quanta $\cdot m^{-2} \cdot s^{-1}$, at 23 °C and 14 h darkness at 18 °C; 50 % relative humidity) for 28–32 days. The plant material was frozen in liquid nitrogen and ground to a fine powder. Total RNA was extracted using an RNA-isolation kit (Promega, Mannheim, Germany) according to the manufacturer's instructions. Following DNase I treatment, cDNA was synthesized from 5 μg of total RNA with MMLV (Moloney-murine-leukaemia virus) RT (reverse transcriptase) II [H-] (Promega) and oligo-dT-priming in 30 μl reactions.

Heterologous expression and site-directed mutagenesis of CYP20-3

CYP20-3 was amplified from *Arabidopsis* cDNA without the N-terminal sequence encoding the signal peptide using Pfu (*Pyrococcus furiosus*) polymerase (Stratagene, La Jolla, CA, U.S.A.). Site-directed mutations were introduced with two subsequent PCRs as described by Montemartini et al. [32]. The primers used for mutagenesis are listed in Supplementary Table S1 (http://www.BiochemJ.org/bj/401/bj4010287add.htm). CYP20-3 cDNA was cloned into the pCR®T7/NT-Topo® vector and transformed into BL21(DE3)pLysS cells (Invitrogen, La Jolla, CA, U.S.A.) for heterologous expression of wild-type and variants of CYP20-3 as His-tagged fusion proteins. The mutations were verified by sequencing.

Culture growth and purification of His-tagged proteins

LB (Luria–Bertani) medium (2 litres) containing 100 μg/ml ampicillin was inoculated with 150 ml of a non-induced overnight bacteria culture and incubated at 37 °C until an attenuance (D) of 0.6–0.8 was obtained at 600 nm using a spectrophotometer (Uvikon 930; Kontron Instruments). Expression of recombinant protein was induced by addition of IPTG (isopropyl 1-thio-β-D-galactopyranoside) to a final concentration of 0.4 mM. After 4 h the cells were harvested by centrifugation (4000 ***g*** for 30 min at 4 °C) and the cell pellet was stored overnight at − 20 °C. Heterologously expressed proteins [CYP20-3_{WT} (where WT is wild-type), CYP20-3_{C54S}, CYP20-3_{C129S}, CYP20-3_{C171S} and CYP20-3_{C176} and CYP20-$3_{\Delta PPI}$] were purified as described previously [33] either under reducing [10 mM 2-mercaptoethanol in lysis buffer (50 mM NaH_2PO_4, 300 mM NaCl and 10 mM imidazol, pH 8.0)] or non-reducing (no reducing reagent added) conditions as indicated. The protein concentrations were determined spectrophotometrically using the Bio-Rad protein assay (Bio-Rad, München, Germany) with BSA as a tentative reference. The protein was stored at − 80 °C. *E. coli* Trx was overexpressed and purified as described by Yamamoto et al. [34] and 2-Cys PrxA, 2-Cys PrxB, PrxII E and PrxQ as described by Horling et al. [22]. Trx-y1 was kindly provided by Dr Emmanuelle Issakidis-Bourguet (Institut de Biotechnologie des Plantes, Université des Paris-Sud, France) and Dr Myroslawa Miginiac-Maslow (Institut de Biotechnologie des Plantes, Université des Paris-Sud, France) [35].

Electrophoretic mobility

A typical assay (50 μl) consisted of 40 mM potassium phosphate buffer (pH 7.0), 1.25 μg of Cyp protein, various concentrations of H_2O_2 and DTT (dithiothreitol) (1–10 mM). Following incubation for 15 min at room temperature (20 °C), the samples were supplemented with equal volumes of 3×-concentrated non-reducing loading buffer [375 mM Tris/HCl, pH 6.8, 30 % (w/v) glycerine, 12 % (w/v) SDS and 0.03 % Bromophenol Blue], and 20 μl aliquots were each separated on SDS/PAGE (16 % gel). Proteins were detected by silver staining.

Excitation and emission spectra of tryptophan fluorescence

Cyp protein (2 μM) dissolved in PBS (pH 7.0) (137.0 mM NaCl, 18.8 mM Na_2HPO_4, 2.7 mM KCl and 2.0 mM KH_2PO_4) was incubated with either 10 mM DTT or 20 mM H_2O_2 for 5 min at room temperature. Excitation and emission spectra were obtained using a spectrofluorimeter (SFM 25; Kontron Instruments). Tryptophan fluorescence was excited at a wavelength of 290 nm and the emission spectrum was recorded as relative fluorescence over the range of 300–400 nm. At least nine independent measurements were carried out for each sample. Data were fitted with the software program FindGraph using an asymmetric Gauss equation.

PPI assay

The PPI assay was performed as described previously [36] with minor modifications. A 1 ml assay consisted of 35 mM Hepes buffer (pH 8.0), 250 μg of α-chymotrypsin (Sigma), 75 nM Cyp, 100 μM *N*-succinyl-Ala-Ala-Pro-Phe-*p*-nitroanilide (Sigma, Deissenhofen, Germany) as chromogenic substrate [10 mM stock solution was dissolved in 100 % (v/v) methanol] and either 10 mM DTT or 2.5 mM H_2O_2. All components of the assay mixture except the α-chymotrypsin were combined and pre-incubated at 10 °C for 10 min. α-Chymotrypsin was added and quickly mixed to initiate the reaction. The absorbance was read every 6 s over a period of 5 min at 390 nm using a spectrophotometer (Uvikon 930; Kontron Instruments). Data were fitted to a first-order rate equation ($A_{360} = A_1 + A_0\ e^{-kt}$, with k as rate constant) and rate constants (k_{obs}) derived as described by Motohashi et al. [31]. The k_{cat}/K_m values were calculated according to the equation $k_{cat}/K_m = (k_{obs} - k_0)/[PPI]$, where k_0 is the first-order rate constant for spontaneous *cis*–*trans* isomerization [37].

Oxidation–reduction midpoint potential

Recombinant CYP20-3 was titrated at pH 7.0. After 3 h incubation in Mops buffer (100 mM) containing 2 mM total DTT (in different ratios of reduced and oxidized DTT) at ambient temperature, the reduced fraction of Cyp was labelled with

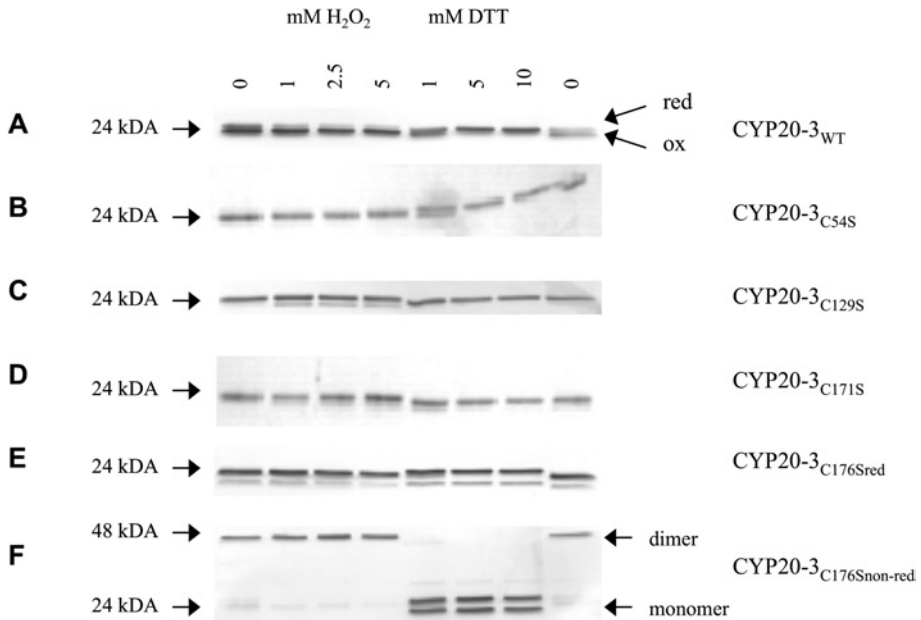

Figure 1 Protein mobility shift of the recombinant Cyp20-3_{WT} and cysteine → serine variants

Cyp (0.5 μg) was incubated with various concentrations of either H_2O_2 or DTT at room temperature for 15 min. All samples were analysed by SDS/PAGE (16 % gel) separation and subsequent silver staining (**A**–**F**).

monobromobimane (10 mM) and analysed for fluorescence [38]. Data were fitted with the software program GraFit5 using the Nernst equation with $n = 4$ (in case of CYP20-3_{WT}) and $n = 3$ (for each mutant protein as one cysteine residue was absent) based on a value of -330 mV for the E_m of DTT at pH 7.0.

DNA-protection assay

CYP20-3-dependent reduction of recombinant chloroplastidic Prx was tested in a DNA-cleavage assay as described previously [21] with minor modifications. ROS (reactive oxygen species) production was induced by incubation of 3 μM $FeCl_3$ in the presence of 10 mM DTT for 3 h at 37 °C. Supercoiled plasmid DNA (pCR®T7/NT-Topo® vector; 2 μg) was added and incubated for 5 h at 37 °C. The reaction mixture contained 6 μg of Prx protein and 3 μg of CYP20-3 or Trx protein as indicated. The *Arabidopsis* peroxiredoxin proteins, 2-Cys PrxA and 2-Cys PrxB, PrxII E and PrxQ [22], were pre-incubated with 5 mM DTT for 5 min followed by incubation with 20 mM H_2O_2 for 1 h, and CYP20-3_{WT} with either 10 mM DTT or 10 mM H_2O_2 for 1 h. The proteins were dialysed overnight against 40 mM potassium phosphate buffer (pH 7.0). Nicking and fragmentation of supercoiled plasmid DNA were monitored by gel electrophoresis in a 1 % agarose gel.

RESULTS

Generation of CYP20-3_{WT} and variants

Site-directed mutations were introduced in the primary amino acid sequence to investigate the functional significance of the cysteine residues in CYP20-3. Overexpressed N-terminally His-tagged CYP20-3_{WT} and variants were isolated and purified by Ni-NTA (Ni^{2+}-nitrilotriacetate) chromatography with yields of 0.25–2 mg/l *E. coli* culture. In non-reducing SDS/PAGE separations, CYP20-3_{WT} and all variants, with the exception of CYP20-3_{C54S}, were detected as reduced monomers after purification under reducing conditions (Figures 1A–1E, lanes 1). CYP20-3_{C176S} revealed a doublet band with a predominant form of lower electrophoretic mobility indicating a partially abnormal conformation, while in wild-type protein, the faster migrating form was abundant. Following purification under non-reducing conditions, CYP20-3_{C176S} was detected as a dimer (Figure 1F).

Redox-dependent electrophoretic mobility of the SDS-solubilized proteins under oxidizing and reducing conditions

As reported by Motohashi et al. [31], two disulfide bonds (Cys^{54}–Cys^{171} and Cys^{129}–Cys^{176}) can be formed in CYP20-3_{WT} that are sensitive to the redox milieu as shown by AMS (4-acetoamido-4′-maleimidyl-stilbene-2,2′-disulfonate)-labelled protein mobility on SDS/PAGE. Thiol–disulfide transitions, e.g. by generating a more compact structure through an intramolecular disulfide bridge formation, often alter apparent electrophoretic mobilities of proteins. Therefore the CYP20-3_{WT} and the diverse variants were checked under oxidizing and reducing conditions. In the presence of H_2O_2, CYP20-3_{WT} showed a higher mobility than after treatment with DTT (Figure 1A). Interestingly, the CYP20-3_{C176S} protein showed aberrant mobility compared with the wild-type and all other cysteine → serine variants. The observed difference in electrophoretic mobility between both monomeric forms was considerably larger than that between the reduced and oxidized forms of the wild-type protein. CYP20-3_{C176S} was partially oxidized after purification, separated as doublet band and showed no further conformational change upon addition of H_2O_2 (Figure 1E). The purification under non-reducing conditions of CYP20-3_{C176S} showed a dimeric form of this variant that converted into the doublet monomeric form upon DTT treatment (Figure 1F). CYP20-3_{C54S} existed in an oxidized and reduced form, but the presence of the oxidized form after purification under reducing conditions indicates that the reduced form is not stable and is highly sensitive to oxidation (Figure 1B). The disulfide bond between Cys^{129} and Cys^{176} forms spontaneously. The deletion of either Cys^{129} or Cys^{176} that forms a disulfide bond in the oxidized protein [31] caused no conformational changes

if purified under reducing conditions. Compared with the wild-type protein CYP20-3_{C171S} is also less sensitive towards H_2O_2, suggesting that no stable disulfide bridge is formed as Cys^{54} sterically inhibits the spontaneous formation of the disulfide bond between Cys^{129} and Cys^{176} (see below, Figure 6A). Formation of a disulfide bond between the adjoining Cys^{54} and Cys^{176} in the tertiary structure can be excluded. In contrast, CYP20-3_{C129S} and CYP20-3_{C171S} were detected mostly in the reduced form and their mobility was not altered under oxidizing conditions (Figures 1C and 1D). This observation indicates that major intramolecular changes associated with the transition from the reduced to the oxidized molecule were absent and probably no disulfide bonds were formed in these variants (Figures 1C and 1D). Apparently, both disulfide bonds are necessary to stabilize the conformation of the oxidized CYP20-3 molecule. These results support the hypothesis that the transition from the reduced to the oxidized form of CYP20-3 as well as the stability of the oxidized form depend on the formation of both disulfide bonds. Furthermore, the two disulfide bonds appear to be formed in a co-ordinated and ordered way.

Intrinsic fluorescence reveals conformational changes during the transition from the reduced to the oxidized state

Analysis of the intrinsic fluorescence offers a powerful approach for studying conformational changes in proteins. The aromatic amino acid tryptophan is rather specifically excited at a wavelength of 290 nm [39]. Burstein et al. [40] introduced two different classes of emission spectra equivalent to different tryptophan locations within the protein structure. The class I-tryptophan is characterized by $\lambda_{em\text{-}max} = 330$–$332$ nm corresponding to a location in the interior of the protein, being shielded from the solvent, whereas class II-tryptophan residues are exposed to the solvent at the protein surface with $\lambda_{em\text{-}max} = 340$–$342$ nm. CYP20-3 contains one tryptophan residue (Trp^{135}) which is part of the RWFH motif and located close to the surface of the protein in the vicinity of Cys^{129} (see Figures 6A and 6B). Emission spectra of CYP20-3_{WT} and its cysteine variants were compared under oxidizing and reducing conditions. For CYP20-3_{WT} a blue shift of $\lambda_{em\text{-}max}$ of 1.6 nm occurred during transition from reducing to oxidizing conditions, indicating that Trp^{135} is more shielded from the solvent in the presence of H_2O_2 (Figure 2A, Table 1). In the presence of DTT, the maximum Trp^{135} fluorescence was blue-shifted in all cysteine → serine variants compared with the wild-type, with the exception of the CYP20-3_{C129S}, whereas in the presence of H_2O_2 the fluorescence maximum was either blue-shifted in CYP20-3_{C54S} and CYP20-3_{C176S} or red-shifted in CYP20-3_{C129S} and CYP20-3_{C171S} (Figure 2, Table 1). Interestingly, the fluorescence emission spectra of the variants mutated in the interacting disulfide bond partners were similar (Figure 2). While $\lambda_{em\text{-}max}$ of CYP20-3_{C54S} and CYP20-3_{C171S} was red-shifted by 2.7 and 2.8 nm respectively upon oxidation, only a slight shift in maximum fluorescence $\lambda_{em\text{-}max}$ was observed for CYP20-3_{C129S} as well as CYP20-3_{C176S} (Figure 2, Table 1). This indicates either an increased exposure of Trp^{135} to the solvent or a stimulated quenching effect of Cys^{129} in the oxidized form. In the case of CYP20-3_{C129S} only a slight shift in the fluorescence maximum by $\lambda_{em\text{-}max} = 344.1$ nm (reduction) and $\lambda_{em\text{-}max} = 344.9$ nm (oxidation) was observed indicating a solvent exposure of the tryptophan [40]. The evidence that Cys^{129} is located in the vicinity of Trp^{135} (see Figures 6A and 6B) together with the observation of the pronounced red shift of $\lambda_{em\text{-}max}$ compared with the wild-type under reducing and oxidizing conditions suggests a strong quenching effect of Cys^{129} on Trp^{135} fluorescence. In conclusion, a major conformational change takes place during the transition from the reduced to the oxidized state, whereby the formation of the disulfide bond between Cys^{54} and Cys^{171} is likely to play a significant role.

The significance of the cysteine residues for the isomerization activity of CYP20-3

CYP20-3 promotes the isomerization of peptidyl-prolyl residues from the *cis*- to the *trans*-form. To investigate the requirement of the conserved cysteine residues for the isomerization activity, wild-type CYP20-3 and the different cysteine variants were analysed for PPI activity. The catalytic efficiency as expressed by the k_{cat}/K_m ratio is derived from the slope of the concentration-dependent k_{obs} values of the corresponding protein. They were determined under reducing and oxidizing conditions respectively (Figure 3, Table 2). The k_{cat}/K_m ratio was $4.23 \times 10^5\ M^{-1} \cdot s^{-1}$ for the reduced form and $1.12 \times 10^5\ M^{-1} \cdot s^{-1}$ for the oxidized form of wild-type CYP20-3 (Figure 3, Table 2) confirming previous reports of oxidation-induced inactivation [31]. Elimination of three out of the four cysteine residues decreased the maximum catalytic PPI activity of the reduced CYP20-3. Activity remained unaltered in the case of CYP20-3_{C176S} (CYP20-3_{C176S}: $k_{cat}/K_m = 3.97 \times 10^5\ M^{-1} \cdot s^{-1}$) (Figure 3, Table 2). Under reducing conditions, the mutation of Cys^{54}, Cys^{129} and Cys^{171} into serine decreased the PPI activity by 60, 51 and 75 % compared with the wild-type respectively. The isomerization activities of the oxidized forms of CYP20-3_{C54S}, CYP20-3_{C129S} and CYP20-3_{C171S} showed no significant differences compared with CYP20-3_{WT}, whereas a significantly higher activity was observed for CYP20-3_{C171S} (Figure 3, Table 2). Moreover, simultaneous mutation of Arg^{69} and Phe^{74}, which are essential amino acids for PPI activity and part of the so-called RWFH motif [3], into Ala^{69} and Leu^{74} respectively abolished the PPI activity (results not shown).

The E_m of CYP20-3_{WT} is -319 mV

The E_m of CYP20-3_{WT} and the variants was determined using a fluorimetric test. The proteins were incubated in redox buffers adjusted with defined ratios of oxidized to reduced DTT, followed by labelling with excess monobromobimane (Figure 4). The wild-type CYP20-3 E_m was determined as -319 ± 2 mV. The E_m values of the cysteine mutants were more negative compared with the wild-type, but only CYP20-3_{C176S} showed a significant decrease (CYP20-3_{C54S}: -320 ± 4 mV, CYP20-3_{C129S}: -326 ± 6 mV, CYP20-3_{C171S}: -322 ± 4 mV and CYP20-3_{C176S}: -326 ± 3 mV; Figure 4).

The residues Cys^{129} and Cys^{171} of CYP20-3 are required for the regeneration of 2-Cys PrxA and 2-Cys PrxB

Recently, Bernier-Villamor et al. [21] showed that the CYP20-3 homologue from *P. sativum* is able to enhance the protective activity of 2-Cys Prx in a DNA-protection assay. The chloroplasts of *A. thaliana* contain four peroxiredoxins, namely 2-Cys PrxA and 2-Cys PrxB, PrxQ and PrxII E [41]. To address the question of whether *Arabidopsis* CYP20-3 is able to specifically reduce Prx, the DNA-protection assay in the presence of DTT/Fe^{3+} was employed with different combinations of CYP20-3 and Prx. In a first set of experiments, CYP20-3_{WT} and the different CYP20-3 variants were tested for their ability to protect the plasmid DNA either directly or by interaction with Prx. Neither reduced nor oxidized CYP20-3_{WT} was able to protect the plasmid DNA (Figure 5A). Likewise, the CYP20-3 variants also showed no protection of DNA (Figure 5B). In a converse manner, CYP20-3_{WT} increased the protective activity in the presence of 2-Cys

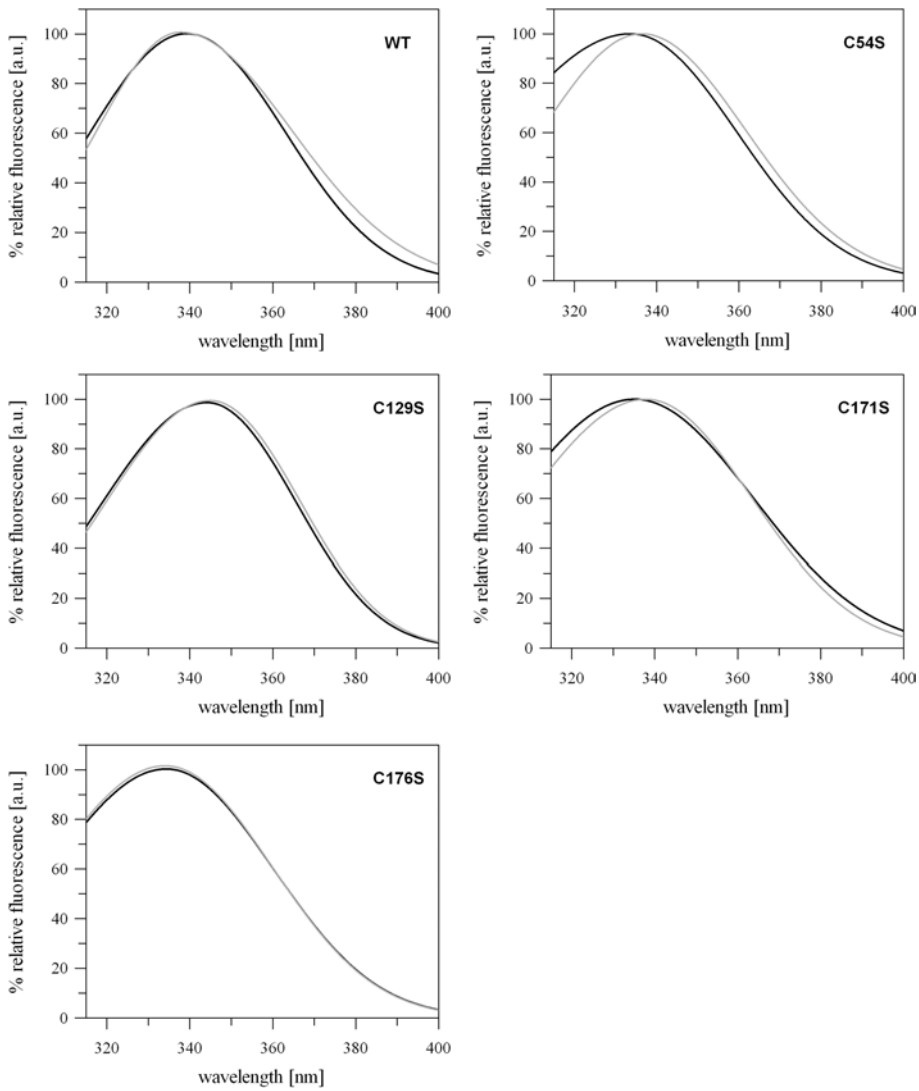

Figure 2 Intrinsic tryptophan fluorescence emission spectra of CYP20-3_{WT} and the cysteine → serine variants as a function of thiol redox state

Tryptophan fluorescence of the proteins was measured under reducing (black line) and oxidizing (grey line) conditions after excitation at $\lambda_{ex} = 290$ nm ($n \geqslant 9$ for each protein). Data were fitted with the software program FindGraph. The wavelengths of the emission maxima ($\lambda_{em\text{-}max}$) are given in Table 1.

Table 1 Emission maximum wavelengths ($\lambda_{em\text{-}max}$) for Cyp20-3_{WT} and the cysteine → serine variants under reducing and oxidizing conditions

Data were fitted by an asymmetric Gaussian equation using the software program FindGraph and analysed for the wavelength of maximum emission. Also given are the calculated differences between the maximum wavelengths of variants minus wild-type under reducing (column 3) and oxidizing conditions (column 5) and the difference between oxidizing and reducing conditions (column 6).

	Reduced		Oxidized		Difference
	$\lambda_{em\text{-}max}$ (nm)	Shift (variant–wt) (nm)	$\lambda_{em\text{-}max}$ (nm)	Shift (variant–wt) (nm)	Oxidized–reduced (nm)
CYP20-3_{WT}	339.2	±0.0	337.6	±0.0	−1.6
CYP20-3_{C54S}	333.7	−5.5	336.4	−1.2	+2.7
CYP20-3_{C129S}	344.1	+4.9	344.9	+7.3	+0.8
CYP20-3_{C171S}	335.2	−4.0	338.0	+0.4	+2.8
CYP20-3_{C176S}	334.4	−4.8	334.1	−3.5	−0.3

PrxA (Figure 5C) and 2-Cys PrxB (Figure 5D). However, no reducing interaction was observed between CYP20-3_{WT} and PrxQ (Figure 5E) or PrxII E (Figure 5F). To prove the functionality of the assay, the DNA protection was tested with known regenerators of PrxQ and 2-Cys PrxB. The results confirmed that 2-Cys Prx is regenerated by *E. coli* Trx [33], and PrxQ by the *A. thaliana* Trx-y_2 [35] respectively, whereas no regenerator for PrxII E was found yet (Figure 5). On a comparative basis, the regeneration of 2-Cys PrxB was more efficient with Trx than with CYP20-3_{WT} (Figure 5D). Until now, the mechanism of the CYP20-3–2-Cys Prx interaction has not been clarified. To identify the cysteines responsible for the reduction of 2-Cys PrxA and 2-Cys PrxB, the different CYP20-3 variants were tested. The addition of the variants CYP20-3_{C54S} and CYP20-3_{C176S} enhanced the fraction of supercoiled DNA and thus showed a better protective activity than the wild-type. The other two cysteine variants had a similar protective pattern compared with the wild-type (Figures 5C and 5D). In conclusion, the cysteine residues Cys^{129} and Cys^{171} are most important for the interaction with 2-Cys PrxA and Cys PrxB.

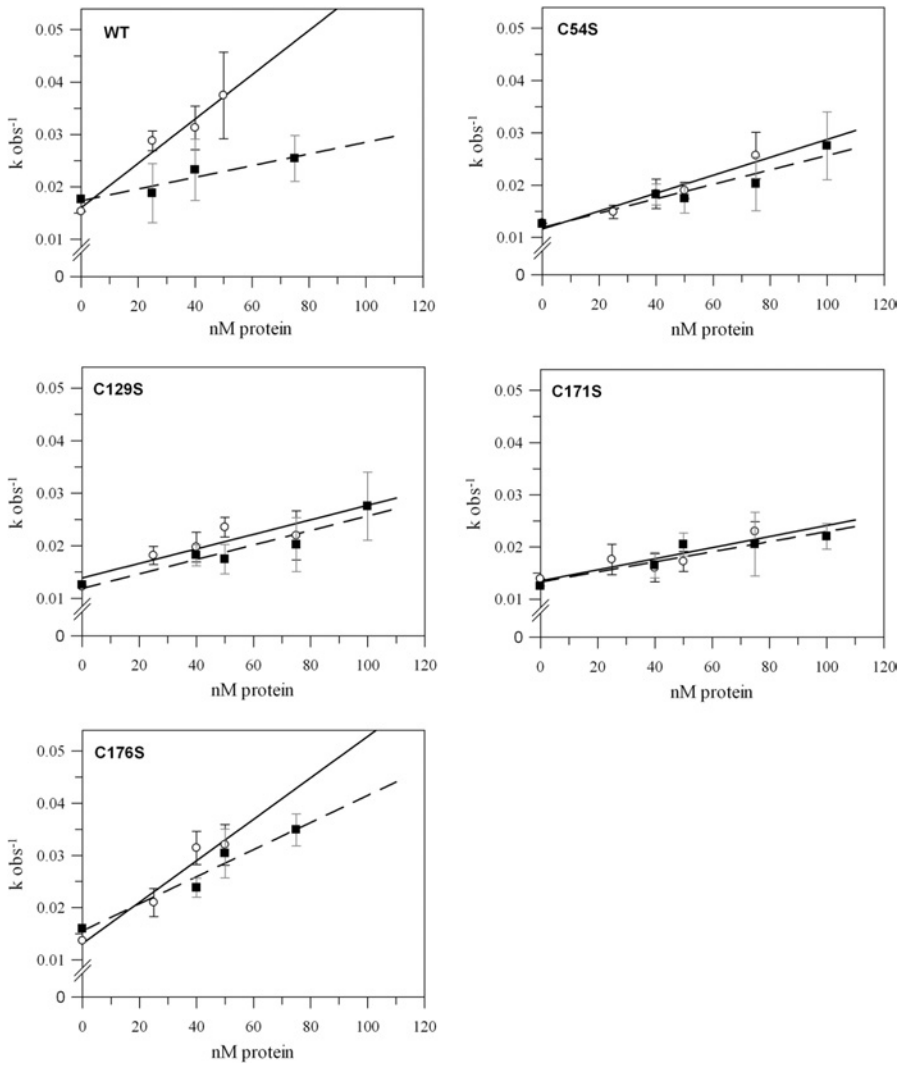

Figure 3 Observed velocity, k_{obs}, with different concentrations of wild-type CYP20-3 and the cysteine → serine variants under reducing or oxidizing conditions

The PPI activity was assayed using *N*-succinyl-Ala-Ala-Pro-Phe-*p*-nitroanilide. Variation of the amount of enzyme led to a family of curves and generated the linear correlation of k_{obs} versus protein concentrations. As described in the Materials and methods section, the slope of each line equals k_{cat}/K_m for the corresponding protein under either reducing or oxidizing conditions as listed in Table 2. The Figure shows the results for wild-type CYP20-3, CYP20-3_{C54S}, CYP20-3_{C129S}, CYP20-3_{C171S} and CYP20-3_{C176S} ($n \geqslant 3$; ± S.D.). Symbols, regression lines and error bars represent reducing and oxidizing conditions as follows: ○, —— and black error bars, 10 mM DTT; ■, - - - and grey error bars, 10 mM H_2O_2 ($n \geqslant 3$; ± S.D.).

Table 2 k_{cat}/K_m values ($s^{-1} \cdot M^{-1}$) for the PPIs of CYP20-3_{WT} and the cysteine → serine variants

Various concentrations of Cyp were incubated with either 10 mM DTT or 10 mM H_2O_2. k_{cat}/K_m values were determined as described in the Materials and methods section.

	Reduced		Oxidized	
	k_{cat}/K_m values ($s^{-1} \cdot M^{-1}$)	(%)	k_{cat}/K_m values ($s^{-1} \cdot M^{-1}$)	(%)
CYP20-3_{WT}	4.23×10^5	100	1.12×10^5	100
CYP20-3_{C54S}	1.71×10^5	40.4	1.38×10^5	123.2
CYP20-3_{C129S}	2.06×10^5	48.7	0.94×10^5	83.9
CYP20-3_{C171S}	1.06×10^5	25.1	0.97×10^5	86.6
CYP20-3_{C176S}	3.97×10^5	93.9	2.59×10^5	231.3

Interestingly, the CYP20-$3_{\Delta PPI}$ variant showed a greater reducing activity than the wild-type protein indicated by the lowest level of plasmid-DNA cleavage (Figures 5C and 5D).

DISCUSSION

CYP20-3 undergoes major conformational changes in dependence on redox state

CYP20-3_{WT} shows altered electrophoretic mobility during the transition from the reduced to the oxidized form when separated under non-reducing conditions by SDS/PAGE (Figure 1A). Motohashi et al. [31] have shown by DTNB labelling and MALDI–TOF MS that oxidized CYP20-3 contains two redox-sensitive disulfide bonds, namely Cys^{54}–Cys^{171} and Cys^{129}–Cys^{176} respectively. The formation of the disulfide bonds Cys^{54}–Cys^{171} and Cys^{129}–Cys^{176} [31] and the two observed redox states of the CYP20-3_{WT} protein (Figure 1A) indicate redox-dependent conformational changes as a basic mechanism for regulating CYP20-3 function. The electrophoretic mobility assays and the intrinsic fluorescence determinations (Figure 2, Table 1) revealed that the transition from the reduced to the oxidized state of CYP20-3 as well as the stability of the oxidized form depend on the formation of both disulfide bonds. In addition, the

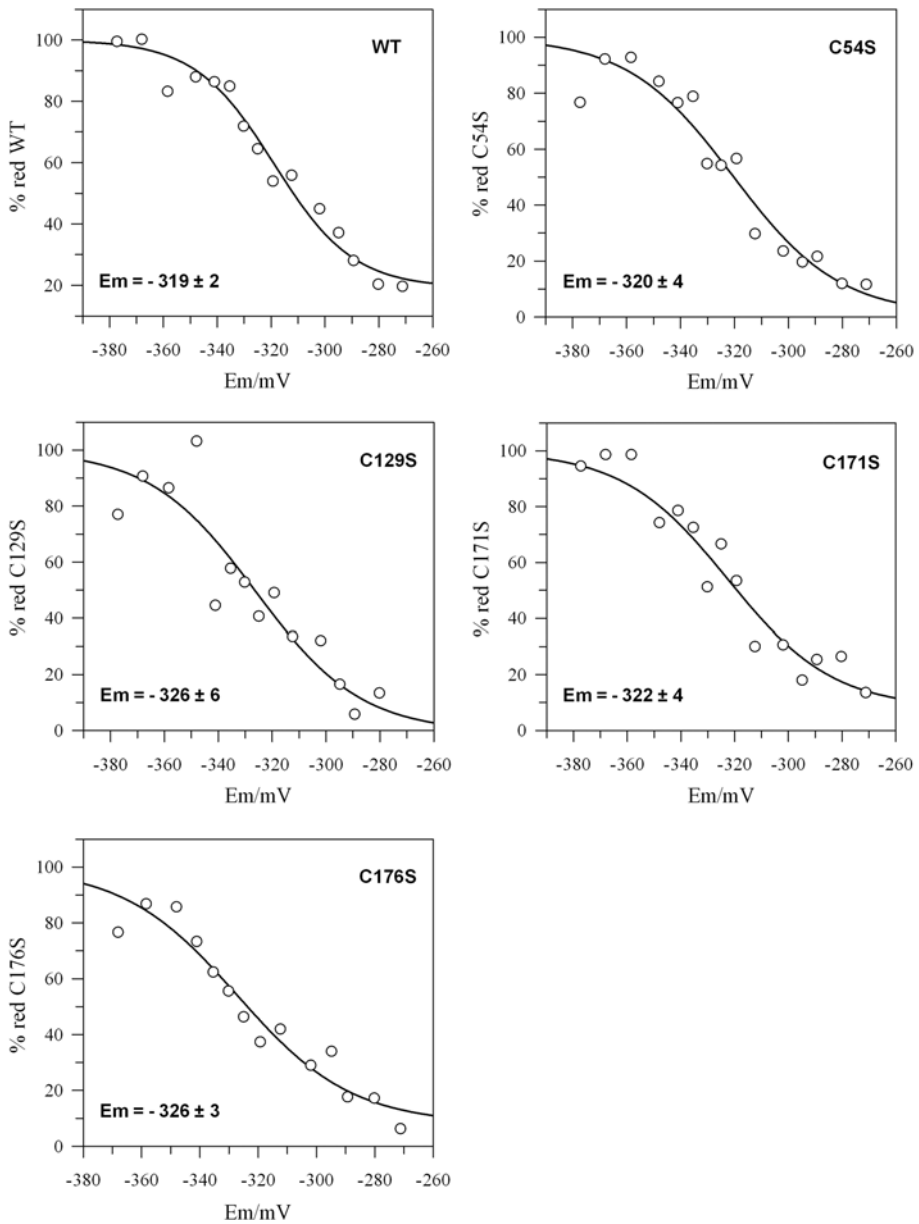

Figure 4 Titration of the E_m values of CYP20-3_{WT} and the cysteine → serine variants

The redox potential of the samples was adjusted by varying the ratio of $DTT_{oxidized}/DTT_{reduced}$. Reduced thiol groups were labelled with monobromobimane and the samples analysed for bound fluorophore. Experimental data were fitted to the Nernst equation with $n = 4$ (wild-type) or $n = 3$ (variants) using GraFit5. E_m values (means ± S.D. for two or more experiments for each protein) are indicated in the Figure.

results from intrinsic fluorescence analysis (Figure 2, Table 1) assign a predominant role in conformational dynamics to the disulfide bridge formation between Cys^{54} and Cys^{171}. The intrinsic fluorescence analysis also confirms that Cys^{54} and Cys^{171}, and Cys^{129} and Cys^{176} co-operate in disulfide bond formation [31] since the corresponding variants revealed identical alterations.

Cysteine residues affect CYP20-3 isomerization activity

CYP20-3 promotes the isomerization of prolyl bonds from the *cis*- to the *trans*-form. The present study provides answers to two redox-related questions, namely: (i) does the isomerization activity depend on the thiol redox state, and (ii) are all cysteine residues equally important with respect to the PPI activity. In accordance with a previous report [31] the isomerization activity of CYP20-3_{WT} was modulated by the redox milieu being less active under oxidizing conditions when disulfide bonds between Cys^{54} and Cys^{171} as well as Cys^{129} and Cys^{176} are formed (Figure 3, Table 2). The k_{cat}/K_m value for reduced CYP20-3_{WT} ($4.23 \times 10^5\ M^{-1} \cdot s^{-1}$) was 6–40-fold lower than previously reported for CYP20-3_{WT} of *A. thaliana* ($8.2 \times 10^6\ M^{-1} \cdot s^{-1}$; [31]), *Caenorhabditis elegans* Cyp3 (CeCyp3) ($k_{cat}/K_m = 2.4 \times 10^6\ M^{-1} \cdot s^{-1}$; [42]) or human CypA (HsCypA) ($1.4 \times 10^7\ M^{-1} \cdot s^{-1}$; [37]). All mutations caused changes regarding the isomerization activity under reducing and oxidizing conditions compared with CYP20-3_{WT}. This implies alterations in the chemical vicinity of the RWFH motif in the variants. The low catalytic efficiency observed in the apparently reduced CYP20-3_{C171S} variant (Figures 1D and 3D, Table 2) supports the conclusion that Cys^{171} is most important to maintain maximum PPI activity.

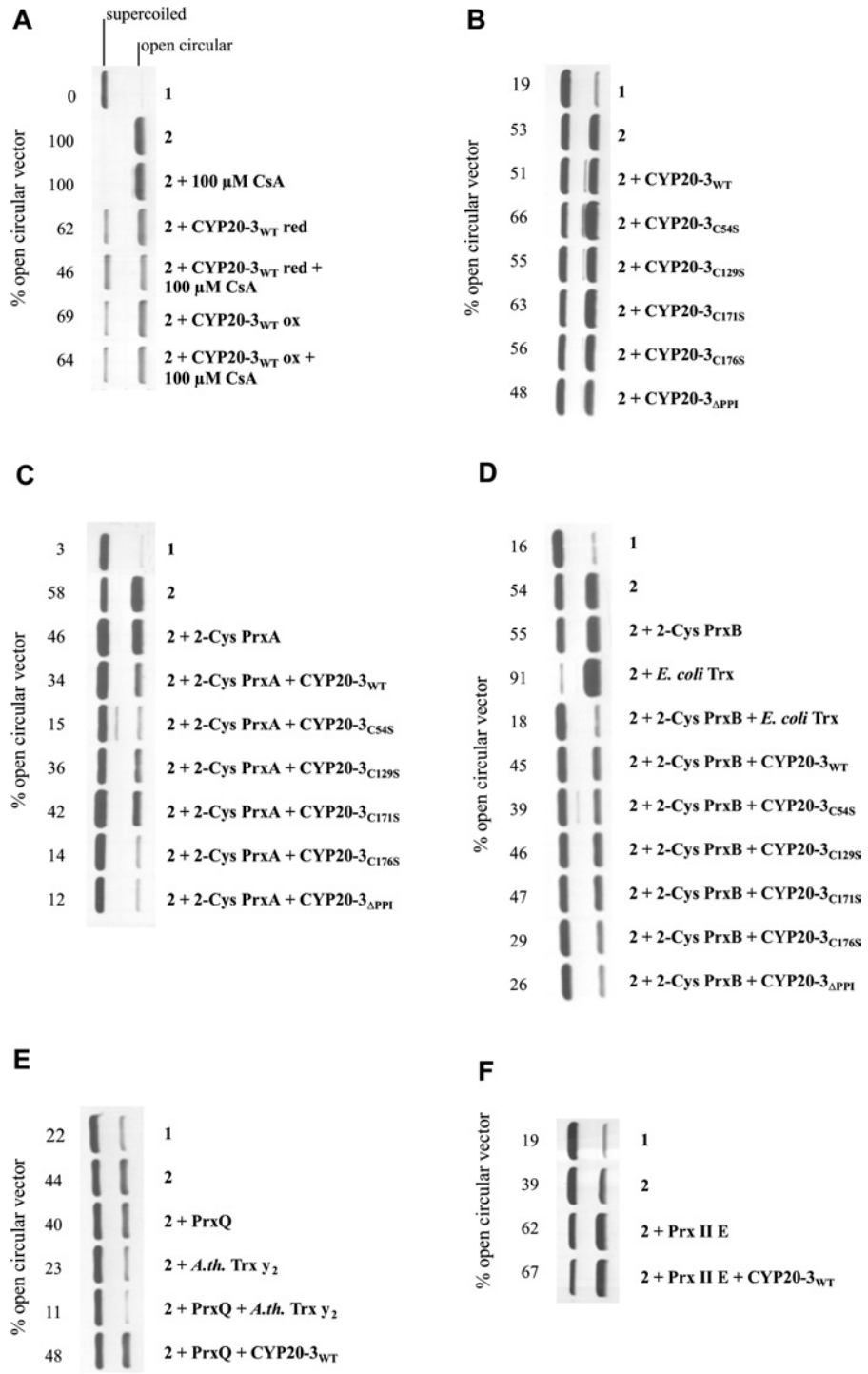

Figure 5 DNA-protection assay as an indicator of CYP20-3-dependent reduction of the chloroplastic Prxs

In each experiment, (1) represents the control without 3 μM $FeCl_3$/10 mM DTT and (2) the maximum cleavage of the plasmid DNA achieved in that particular experiment with 3 μM $FeCl_3$/10 mM DTT but without added protein. (**A**) Effect of CYP20-3 redox state and CsA on DNA cleavage in the absence of Prx. (**B**) Effect of CYP20-3 and the different cysteine → serine variants (each 3 μg) on DNA cleavage. (**C**) Effect of CYP20-3 and cysteine → serine variants (each 3 μg) on 2-Cys PrxA (6 μg)-mediated DNA protection. (**D**) Effect of CYP20-3 and cysteine → serine variants (each 3 μg) on 2-Cys PrxB-mediated DNA protection. Thioredoxin was added as an efficient donor control. (**E**) Effect of CYP20-3 on PrxQ-dependent DNA protection (6 μg). (**F**) Effect of CYP20-3 on PrxII E-dependent DNA protection. The percentage of open circular plasmid DNA, indicating ROS-mediated cleavage, is given for each experiment. Each experiment was performed three or more times with similar results.

The wild-type-like catalytic activity of reduced CYP20-3_{C176S} on the other hand indicates a minor role in PPI activity, but a major role in oxidative inactivation since CYP20-3_{C176S} maintained a very high catalytic efficiency. The thiol-dependency of CYP20-3 PPI activity contrasts the insensitivity of HsCypA PPI to mutation of the residues Cys^{52}, Cys^{62}, Cys^{115} and Cys^{161} [37] although

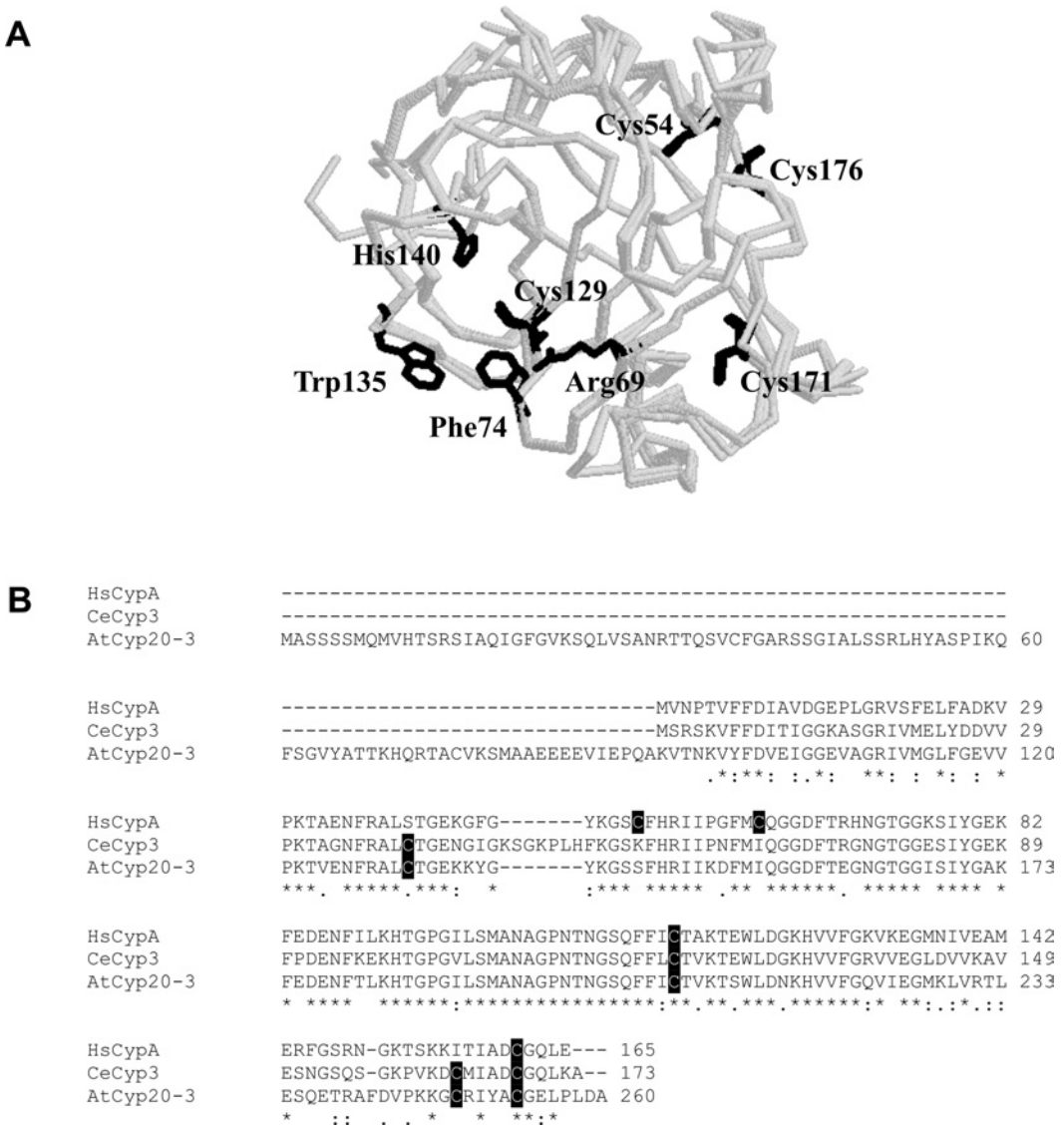

Figure 6 Structure and amino acid sequence alignment of CYP20-3

(**A**) Localization of the residues Cys[54], Cys[129], Cys[171] and Cys [176] as well as Trp[135] in the tertiary structure and in comparison with the active centre represented by the RFWH motif of the CYP20-3 molecule. The Cys[54] and Cys[176] are arranged very close together in the structure of CYP20-3 and are part of the surface of the molecule, therefore possibly being accessible to ROS. The Cys[129] and Cys[171] are located on the opposite site of the molecule compared with Cys[54] and Cys[176]. The model was calculated based on known structures of human CypB and Cyp3 from *C. elegans* respectively using Deep View/Swiss-Pdb Viewer 3.7 (http://www.expasy.org/spdbw/) and further processed by using Rasmol. (**B**) Amino acid sequence alignment of the *A. thaliana* Cyp CYP20-3 (GenBank® B53422, without the signal peptide of 77 amino acids), CypA from *H. sapiens* (GenBank® P62937) and Cyp3 from *C. elegans* (GenBank® NP_506751). The conserved cysteine residues are shaded and the catalytic motif of a typical PPI is underlined.

two of the four cysteine residues of HsCypA are located within the PPI motif. Interestingly, only Cys[129] and Cys[176] are conserved between plant and human Cyp, whereas Cys[54] and Cys[171] in the plant protein are absent from the human protein (Figure 6B). Accordingly, the disulfide bridge between Cys[54] and Cys[171] is essential for the redox control of the PPI activity.

Importance of the disufide bonds

The E_m of CYP20-3_{WT} was determined to be -319 ± 2 mV (Figure 4). The E_m values of the variants were similar to that of the wild-type. It may be postulated that the oxidation of one disulfide bond alters the redox potential of the second disulfide bond causing an easier/faster oxidation. However, it was impossible to determine the E_m values for each disulfide bond independently. The variants CYP20-3_{C54S} (-320 mV) and CYP20-3_{C171S} (-322 mV) have a slightly less negative redox potential than the other two variants (CYP20-3_{C129S}: -326 mV and CYP20-3_{C176S}: -326 mV). In the variants CYP20-3_{C54S} and CYP20-3_{C171S} the E_m of the disulfide bridge between Cys[129] and Cys[176] is less negative indicating an easier reduction. In a converse manner, the disulfide bridge between Cys[54] and Cys[171] is more easily formed than the disulfide bridge between Cys[129] and Cys[176]. This interpretation is still speculative in the light of the similarity and the standard deviation of the determined E_m values. However, this hypothesis fits into the emerging picture that the disulfide bond between Cys[54] and Cys[171] is the more important one for the redox properties of functional CYP20-3. These two cysteine

residues are conserved in other *Arabidopsis* Cyps. It will have to be tested whether these proteins also are regulated by thiol–disulfide transition. On the other hand, amino acids corresponding to Cys^{176} lack in all other members of the *Arabidopsis* Cyp protein family [3].

CYP20-3 as regenerator of chloroplast peroxiredoxins

The E_m of CYP20-3_{WT} (−319 mV) was more negative than that of 2-Cys PrxA (−307 mV) [33]. Reductive activation of CYP20-3 is likely to occur under conditions of excess electron pressure in photosynthesis. In accordance with other publications, *in vitro* experiments revealed Trx-m as an interaction partner of CYP20-3: Trx-m with an E_m of −300 mV is able to reduce CYP20-3 and to activate its PPI activity [30,31,43]. Previously, Lee et al. [20] reported that HsCypA activates human Prx, and Bernier-Villamor et al. [21] showed that a CYP20-3 homologue from *P. sativum* supports the peroxide-detoxifying activity of plant 2-Cys Prx. The E_m values of chloroplast Prxs range between −290 mV for PrxII E, −307 mV for 2-Cys Prx A, −322 mV for 2-Cys Prx B and −325 mV for PrxQ [22,44]. Thus, based on redox potentials, all chloroplast Prxs are potential targets for CYP20-3, considering that an efficient reduction of the regulatory disulfides still can occur in the presence of a ΔE_m of up to 20 mV [44]. The DNA-protection assay manifested the ability of CYP20-3 to reduce 2-Cys PrxA and 2-Cys PrxB (Figure 5) similar to *E. coli* Trx [33] and *Arabidopsis* Trx-m, -y1, -y2 and -x [35]. In a converse manner, the combination of PrxII E and PrxQ respectively in combination with CYP20-3 gave no protection of plasmid DNA in the DNA-cleavage assay (Figures 5E and 5F). It is concluded that CYP20-3 is unable to reduce PrxQ and PrxII E efficiently. This suggests that 2-Cys PrxA and 2-Cys PrxB are specific interaction partners of CYP20-3 at least *in vitro*.

The redox-dependent properties of Cyps may also be relevant in other organisms. CeCyp3 that shows a similarity at the protein primary sequence level of 63 % to CYP20-3 possesses four cysteine residues at conserved positions homologous with the four in CYP20-3 suggesting similar function (Figure 6B) [42]. The authors proposed that CeCyp3 might play a role in a signalling response to oxidative stress.

The DNA-cleavage assay proved Prx-reducing activity of all four variants, but the particular importance of Cys^{129} and Cys^{171} in the reduction of 2-Cys PrxA and 2-Cys PrxB (Figures 5C and 5D). Lee et al. [20] found Cys^{115} and Cys^{161} of human CypA corresponding to Cys^{129} and Cys^{176} of CYP20-3 (Figure 6B) to be important for the reduction of human PrxII using the glutamine synthetase protection assay. Taking together the results of the PPI activity measurements (Figure 3) and the DNA-protection assay (Figure 5) suggest that Cys^{171} is involved in both redox-related functions. The CYP20-$3_{\Delta PPI}$ variant showed an increased reducing activity towards 2-Cys PrxA and 2-Cys PrxB (Figures 5C and 5D) implying that Cys^{129} or Cys^{171} is better accessible for oxidized 2-Cys PrxA and 2-Cys PrxB after changing the thiols in close vicinity of the active centre. As the CYP20-$3_{\Delta PPI}$ variant showed no PPI activity (results not shown), but greater reducing activity, it can be concluded that both functions of CYP20-3, i.e. the catalytic activity as PPI and the function as reductant, are independent from each other. Nevertheless, both functions are regulated in dependence on the redox status of the active centre of CYP20-3. The best-known mechanism to modify Cyp activity is the binding of CsA, an immunosuppressive drug that specifically inhibits the Cyp PPI activity [4]. Subsequently, the CsA–Cyp complex binds to subunit B of the Ca^{2+}/calmodulin-dependent serine/threonine-phosphatase calcineurin leading to its inactivation and, finally, resulting in altered gene transcription in the nucleus [45,46]. Thus the electron-donating property of CYP20-3 to 2-Cys Prx as observed in the DNA-protection assay does not necessarily indicate a major role of CYP20-3 in the antioxidant defence of the chloroplast, but does indicate a role in the redox signalling network adjusting the redox state and thereby the activity of CYP20-3. In this scenario, the 2-Cys Prx serves as a peroxide sensor transmitting redox information to CYP20-3 that in turn modulates target protein functions [47]. It will be necessary to identify other interacting partners and thus regulatory targets of CYP20-3. Furthermore, the analysis of *Arabidopsis* lines lacking or overexpressing CYP20-3 protein will possibly allow clarifying its physiological role within the plant redox network in the adaptation process to stress.

Expert technical assistance by Heike Bogunovic is gratefully acknowledged. Trx-y1 was kindly provided by Dr Emmanuelle Issakidis-Bourguet (Institut de Biotechnologie des Plantes, Université des Paris-Sud, France) and Dr Myroslawa Miginiac-Maslow (Institut de Biotechnologie des Plantes, Université des Paris-Sud, France). We thank Dr Andreas Brockhinke (Faculty of Chemistry, Bielefeld University, Bielefeld, Germany) for helpful discussion. Research was supported by Bielefeld University within the FIF (Forschungs- und Innovationsfond)-initiative and by the Deutsche Forschungsgemeinschaft within the SFB (Sonderforschungsbereich) 613 (D9), but also FOR (Forschergruppe) 387 (TP3).

REFERENCES

1 He, Z., Li, L. and Luan, S. (2004) Immunophilins and parvulins. Superfamily of peptidyl prolyl isomerases in *Arabidopsis*. Plant Physiol. **134**, 1248–1267
2 Buchanan, B. B. and Luan, S. (2005) Redox regulation in the chloroplast thylakoid lumen: a new frontier in photosynthesis research. J. Exp. Bot. **56**, 1439–1447
3 Romano, P. G. N., Horton, P. and Gray, J. E. (2004) The *Arabidopsis* cyclophilin gene family. Plant Physiol. **134**, 1268–1282
4 Handschumacher, R. E., Harding, M. W., Rice, J. and Drugge, R. J. (1984) Cyclophilin: a specific cytosolic binding protein for cyclosporin A. Science **226**, 544–547
5 Romano, P. G. N., Gray, J., Horton, P. and Luan, S. (2005) Plant immunophilins: functional versatility beyond protein maturation. New Phytol. **166**, 753–769
6 Bächinger, H. P. (1987) The influence of peptidyl-prolyl *cis–trans* isomerase on the *in vitro* folding of type III collagen. J. Biol. Chem. **262**, 17144–17148
7 Davis, J. M., Boswell, B. A. and Bächinger, H. P. (1989) Thermal stability and folding of type IV procollagen and effect of peptidyl-prolyl *cis–trans*-isomerase on the folding of the triple helix. J. Biol. Chem. **264**, 8956–8962
8 Schönbrunner, E. R. and Schmid, F. X. (1992) Peptidyl-prolyl *cis–trans* isomerases improve the efficiency of protein disulfide isomerase as a catalyst of protein folding. Proc. Natl. Acad. Sci. U.S.A. **89**, 4510–4513
9 Gupta, R., Mould, R. M., He, Z. and Luan, S. (2002) A chloroplast FKBP interacts with and affects the accumulation of Rieske subunit of cytochrome b_f complex. Proc. Natl. Acad. Sci. U.S.A. **99**, 15806–15811
10 Freskgard, P. O., Bergenhem, N., Johnsson, B. H., Svensson, M. and Carlsson, U. (1992) Isomerase and chaperone activity of prolyl isomerase in the folding of carbonic anhydrase. Science **258**, 466–468
11 Freeman, B. C., Toft, D. O. and Morimoto, R. I. (1996) Molecular chaperone machines: chaperone activities of the Cyp-40 and the steroid aporeceptor associated protein p23. Science **274**, 1718–1720
12 Maleszka, R., Lupas, A., Hanes, S. D. and Miklos, G. L. (1997) The dodo gene family encodes a novel protein involved in signal transduction and protein folding. Gene **203**, 89–93
13 Brazin, K. N., Mallis, R. J., Fulton, D. B. and Andreotti, A. H. (2001) Regulation of the tyrosine kinase Itk by the peptidyl-prolyl isomerase cyclophilin A. Proc. Natl. Acad. Sci. U.S.A. **99**, 1899–1904
14 Jin, Z.-G., Melaragno, M. G., Liao, D.-F., Yan, C., Haendeler, J., Suh, Y.-A, Lambeth, J. D. and Berk, B. C. (2000) Cyclophilin A is a secreted growth factor induced by oxidative stress. Circ. Res. **87**, 789–796
15 Luan S., Lane W. S. and Schreiber, S.L. (1994) pCyP B: a chloroplast-localized, heat shock-responsive cyclophilin from fava bean. Plant Cell **6**, 885–892
16 Meza-Zepeda, L. A., Baudo, M. M., Palva, E. T. and Heino, P. (1998) Isolation and characterization of a cDNA corresponding to a stress-activated cyclophilin gene in *Solanum commersonii*. J. Exp. Bot. **49**, 1451–1452

17 Berardini, T. Z., Bollmann, K., Sun, H. and Poethig, R. S. (2001) Regulation of vegetative phase change in *Arabidopsis thaliana* by cyclophilin 40. Science **291**, 2405–2407
18 Horowitz, D. S., Lee, E. J., Mabon, S. A. and Misteli, T. (2002) A cyclophilin function in pre-mRNA splicing. EMBO J. **21**, 470–480
19 Ingelfinger, D., Göthel, S. F., Marahiel, M. A., Reidt, U., Ficner, R., Lührmann, R. and Achsel, T. (2003) Two protein-protein interaction sites on the spliceosome-associated human cyclophilin CypH. Nucleic Acids Res. **31**, 4791–4796
20 Lee, S. P., Hwang, Y. S., Kim, Y. J., Kwon, K.-S., Kim, H. J., Kim, K. and Chae, H. Z. (2001) Cyclophilin A binds to peroxiredoxins and activates its peroxidase activity. J. Biol. Chem. **276**, 29826–29832
21 Bernier-Villamor, L., Navarro, E., Sevilla, F. and Lázaro, J.-J. (2004) Cloning and characterization of a 2-Cys peroxiredoxin from *Pisum sativum*. J. Exp. Bot. **55**, 2191–2199
22 Horling, F., Lamkemeyer, P., König, J., Finkemeier, I., Kandlbinder, A., Baier, M. and Dietz, K.-J. (2003) Divergent light-, ascorbate-, and oxidative stress-dependent regulation of expression of the peroxiredoxin gene family in *Arabidopsis*. Plant Physiol. **131**, 317–325
23 Hofmann, B., Hecht, H. J. and Flohe, L. (2002) Peroxiredoxins. J. Biol. Chem. **383**, 347–364
24 König, J., Lotte, K., Plessow, R., Brockhinke, A., Baier, M. and Dietz, K.-J. (2003) Reaction mechanism of plant 2-Cys peroxiredoxin: role of the C-terminus and the quaternary structure. J. Biol. Chem. **278**, 24409–24420
25 Dietz, K.-J. (2003) Plant peroxiredoxins. Annu. Rev. Plant Biol. **54**, 93–107
26 Dietz, K.-J., Jacob, S., Oelze, M.-L., Laxa, M., Tognetti, V., de Miranda, S. M., Baier, M. and Finkemeier, I. (2006) The function of peroxiredoxins in plant organelle redox metabolism. J. Exp. Bot. **57**, 1697–1709
27 Finkemeier, I., Goodman, M., Lamkemeyer, P., Kandlbinder, A., Sweetlove, L. J. and Dietz, K.-J. (2005) The mitochondrial type II peroxiredoxin F is essential for redox homeostasis and root growth of *Arabidopsis thaliana* under stress. J. Biol. Chem. **280**, 12168–12180
28 Lippuner, V., Chou, I. T., Scott, S. V., Ettinger, W. F., Theg, S. M. and Gasser, C. S. (1994) Cloning and characterization of chloroplast and cytosolic forms of cyclophilin from *Arabidopsis thaliana*. J. Biol. Chem. **269**, 7863–7868
29 Schubert, M., Petersson, U. A., Haas, B. J., Funk, C., Schröder, W. P. and Kieselbach, T. (2002) Proteome map of the chloroplast lumen of *Arabidopsis thaliana*. J. Biol. Chem. **277**, 8354–8365
30 Motohashi, K., Kondoh, A., Stumpp, M. T. and Hisabori, T. (2001) Comprehensive survey of proteins targeted by chloroplast thioredoxin. Proc. Natl. Acad. Sci. U.S.A. **98**, 11224–11229
31 Motohashi, K., Koyama, F., Nakanishi, Y., Ueoka-Nakanishi, H. and Hisabori, T. (2003) Chloroplast cyclophilin is a target protein of thioredoxin. J. Biol. Chem. **278**, 31848–31852
32 Montemartini, M., Kalisz, H. M., Hecht, H. J., Steinert, P. and Flohe, L. (1999) Activation of active-site cysteine residues in the peroxiredoxin-type tryparedoxin peroxidase of *Crithidia fasciculata*. Eur. J. Biochem. **264**, 516–524

Received 18 July 2006/22 August 2006; accepted 24 August 2006
Published as BJ Immediate Publication 24 August 2006, doi:10.1042/BJ20061092

33 König, J., Baier, M., Horling, F., Kahmann, U., Harris, G., Schürmann, P. and Dietz, K.-J. (2002) The plant-specific function of 2-Cys peroxiredoxin-mediated detoxification of peroxides in the redox-hierachy of photosynthetic electron flux. Proc. Natl. Acad. Sci. U.S.A. **99**, 5738–5743
34 Yamamoto, H., Miyake, C., Dietz, K.-J., Tomizawa, K.-I., Murata, N. and Yokota, A. (1999) Thioredoxin peroxidase in the cyanobacterium *Synechocystis* sp. PCC 6803. FEBS Lett. **447**, 269–273
35 Collin, V., Lamkemeyer, P., Miginiac-Maslow, M., Hirasawa, M., Knaff, B. D., Dietz, K.-J. and Issakidis-Bourguet, E. (2004) Characterization of plastidial thioredoxins from *Arabidopsis* belonging to the new y-type1. Plant Physiol. **136**, 4088–4095
36 Fischer, G., Bang, H., Berger, E. and Schellenberger, A. (1984) Conformational specificity of chymotrypsin toward proline-containing substrates. Biochim. Biophys. Acta **791**, 87–97
37 Liu, J., Albers, M. W., Chen, C.-M., Schreiber, S. L. and Walsh, C. T. (1990) Cloning, expression, and purification of human cyclophilin in *Escherichia coli* and assessment of the catalytic role of cysteines by site-directed mutagenesis. Proc. Natl. Acad. Sci. U.S.A. **87**, 2304–2308
38 Hirasawa, M., Schürmann, P., Jacquot, J.-P., Manieri, W., Jacquot, P., Keryer, E., Hartman, F. C. and Knaff, D. B. (1999) Oxidation-reduction properties of chloroplast thioredoxins, ferredoxin: thioredoxin reductase, and thioredoxin f-regulated enzymes. Biochemistry **38**, 5200–5205
39 Teale, F. W. J. and Weber, G. (1957) Ultraviolet fluorescence of the aromatic amino acids. Biochem. J. **65**, 476–482
40 Burstein, E. A., Vedenkins, N. S. and Ivkova, M. N. (1973) Fluorescence and the location of tryptophan residues in protein molecules. Photochem. Photobiol. **18**, 263–279
41 Dietz, K.-J., Horling, F., König, J. and Baier, M. (2002) The function of the chloroplast 2-cysteine peroxiredoxin in peroxide detoxification and its regulation. J. Exp. Bot. **53**, 1321–1329
42 Dornan, J., Page, A. P., Taylor, P., Wu, S.-Y., Winter, A. D., Husi, H. and Walkinshaw, M. D. (1999) Biochemical and structural characterization of a divergent loop cyclophilin from *Caenorhabditis elegans*. J. Biol. Chem. **274**, 34877–34883
43 Hisabori, T., Hara, S., Fujii, T., Yamazaki, D., Hosoya-Matsuda, N. and Motohashi, K. (2005) Thioredoxin affinity chromatography: a useful method for further understanding the thioredoxin network. J. Exp. Bot. **56**, 1463–1468
44 Rouhier, N., Gelhaye, E., Gualberto, J. M., Jordy, M.-N., De Faye, E., Hirasawa, M., Duplessis, S., Lemaire, S. D., Frey, P., Martin, F. et al. (2004) Poplar peroxiredoxin Q. A thioredoxin-linked antioxidant functional in pathogen defense. Plant Physiol. **134**, 1027–1038
45 Liu, J., Farmer, J. D., Lane, W. S., Friedman, J., Weissman, I. and Schreiber, S. L. (1991) Calcineurin is a common target of cyclophilin–cyclosporin A and FKBP–FK506 complexes. Cell **66**, 807–815
46 Li, W. and Handschumacher, R. E. (1993) Specific interaction of the cyclophilin–cyclosporin complex with the B subunit of calcineurin. J. Biol. Chem. **268**, 14040–14044
47 Dietz, K. J. (2003) Redox regulation, redox signalling and redox homeostasis in plant cells. Intern. Rev. Cytol. **228**, 141–193